RASA1 functions in EPHB4 signaling pathway to suppress endothelial mTORC1 activity

Jun Kawasaki, … , Steven J. Fishman, Joanne Chan

Research Article   Vascular biology

Vascular malformations are linked to mutations in RAS p21 protein activator 1 (*RASA1*, also known as *p120RasGAP*); however, due to the global expression of this gene, it is unclear how these mutations specifically affect the vasculature. Here, we tested the hypothesis that RASA1 performs a critical effector function downstream of the endothelial receptor EPHB4. In zebrafish models, we found that either RASA1 or EPHB4 deficiency induced strikingly similar abnormalities in blood vessel formation and function. Expression of WT EPHB4 receptor or engineered receptors with altered RASA1 binding revealed that the ability of EPHB4 to recruit RASA1 is required to restore blood flow in EPHB4-deficient animals. Analysis of EPHB4-deficient zebrafish tissue lysates revealed that mTORC1 is robustly overactivated, and pharmacological inhibition of mTORC1 in these animals rescued both vessel structure and function. Furthermore, overexpression of mTORC1 in endothelial cells exacerbated vascular phenotypes in animals with reduced EPHB4 or RASA1, suggesting a functional EPHB4/RASA1/mTORC1 signaling axis in endothelial cells. Tissue samples from patients with arteriovenous malformations displayed strong endothelial phospho-S6 staining, indicating increased mTORC1 activity. These results indicate that deregulation of EPHB4/RASA1/mTORC1 signaling in endothelial cells promotes vascular malformation and suggest that mTORC1 inhibitors, many of which are approved for the treatment of certain cancers, should be further explored as a potential strategy to treat patients with vascular malformations.

Find the latest version:

https://jci.me/67084/pdf

RASA1 functions in EPHB4 signaling pathway to suppress endothelial mTORC1 activity

Jun Kawasaki,[1] Sandrine Aegerter,[1] R. Dawn Fevurly,[1,2] Akiko Mammoto,[1]
Tadanori Mammoto,[1] Mustafa Sahin,[3] John D. Mably,[4] Steven J. Fishman,[2] and Joanne Chan[1]

[1]Vascular Biology Program, Department of Surgery, [2]Vascular Anomalies Center, Department of Surgery,
[3]The F.M. Kirby Neurobiology Center, Department of Neurology, and [4]Department of Cardiology, Department of Genetics,
Boston Children's Hospital, Harvard Medical School, Boston, Massachusetts, USA.

Vascular malformations are linked to mutations in RAS p21 protein activator 1 (*RASA1*, also known as *p120RasGAP*); however, due to the global expression of this gene, it is unclear how these mutations specifically affect the vasculature. Here, we tested the hypothesis that RASA1 performs a critical effector function downstream of the endothelial receptor EPHB4. In zebrafish models, we found that either RASA1 or EPHB4 deficiency induced strikingly similar abnormalities in blood vessel formation and function. Expression of WT EPHB4 receptor or engineered receptors with altered RASA1 binding revealed that the ability of EPHB4 to recruit RASA1 is required to restore blood flow in EPHB4-deficient animals. Analysis of EPHB4-deficient zebrafish tissue lysates revealed that mTORC1 is robustly overactivated, and pharmacological inhibition of mTORC1 in these animals rescued both vessel structure and function. Furthermore, overexpression of mTORC1 in endothelial cells exacerbated vascular phenotypes in animals with reduced EPHB4 or RASA1, suggesting a functional EPHB4/RASA1/mTORC1 signaling axis in endothelial cells. Tissue samples from patients with arteriovenous malformations displayed strong endothelial phospho-S6 staining, indicating increased mTORC1 activity. These results indicate that deregulation of EPHB4/RASA1/mTORC1 signaling in endothelial cells promotes vascular malformation and suggest that mTORC1 inhibitors, many of which are approved for the treatment of certain cancers, should be further explored as a potential strategy to treat patients with vascular malformations.

Introduction

Vascular anomalies encompass a large number of blood and lymphatic vessel disorders that are typically diagnosed during childhood or sometimes by routine prenatal ultrasound screening (1). These primary vascular diseases can be generally divided into vascular tumors, such as hemangiomas, and vascular malformations, such as capillary, venous, arteriovenous, or lymphatic malformations (2–4). Limited treatment options are currently available. Thus, understanding the molecular mechanisms that drive the formation of these lesions could provide a strong foundation for developing targeted therapies. Genetic linkage defined RAS p21 protein activator 1 (*RASA1*; also known as *p120-RasGAP*) as the causative gene in an autosomal dominant form of vascular malformation, known as capillary malformation–arteriovenous malformation (CM-AVM; refs. 5–7). Inactivating mutations in a single allele of *RASA1* was sufficient to cause CM-AVM (5); however, the severity of disease presentation is quite variable (6, 8, 9). While some patients have mild to no symptoms, others have vascular lesions that are in danger of rupture. Typically, high-risk lesions are either embolized and/or surgically resected; however, owing to the underlying genetic nature of this vascular disease, the frequency of recurrence is high (10). CM-AVM patients could also have vascular malformations that are not amenable to treatment, which then become a lifelong ailment. Since *RASA1* is widely expressed in many tissues and cell types (11), how mutations in this gene cause localized, vascular-specific abnormalities is unknown (3, 5, 12).

RASA1 is best known as a negative regulator of RAS through its GTPase activating protein (GAP) activity (13). Thus, a link between

RAS regulation and CM-AVM progression is a likely possibility, but the precise molecular players involved are not yet understood (3, 5, 12). Oncogenic *RAS* mutations are found in a large number of human cancers. These mutations usually provide resistance toward RASGAPs, so that oncogenic RAS remains constitutively activated within cancer cells (14). For this reason, early studies postulated that loss-of-function mutations in *RASA1*, particularly in its GAP domain, might also occur at a high frequency in human cancers. However, this was not the case. Only 3 mutations in *RASA1*'s GAP domain were found among 188 human tumor samples (15). None were found among 53 human lung cancer cell lines (16).

To investigate the in vivo functions of RASA1, 3 genetic mouse models have been generated. The first was a *Rasa1*-null mouse, published in 1995, which exhibited widespread neuronal cell death, vascular disorganization, and embryonic lethality by E10.5. Meanwhile heterozygotes were phenotypically normal and viable (11). In a recent study, inducible or endothelial-specific *Rasa1*-knockout mice were generated and carefully analyzed by Lapinski et al. (17). Similar to the *Rasa1*-null model, endothelial-specific *Rasa1*-knockout mice were also embryonic lethal at the same stage (11, 17). Using the inducible mouse model, the authors discovered a role for RASA1 in lymphatic vessel formation when systemic knockout was carried out at 2 or more months of postnatal life (17). Despite careful analysis, however, no CMs or AVMs were found in any tissue. Conversely, in humans with inactivating mutations in 1 allele of *RASA1*, the occurrence of lymphatic lesions is rare in comparison with vascular malformations (9, 17).

The RASA1/p120RasGAP protein has been shown to interact with a number of activated receptor tyrosine kinases (RTKs), including EGF, PDGF, and EPH receptors (18–20). Among the EPH family, the EPHB4 receptor plays a unique role in vascular

development, where it regulates arteriovenous differentiation (21, 22). Early studies on ephrin-B2– and *Ephb4*-null mice provided the first in vivo evidence for the existence of a genetic program governing the distinction between arteries and veins, even before the onset of blood flow (21–23). Since then, upstream genes that can regulate EPHB4 or ephrin-B2 expression have been defined to further delineate the genes involved in regulating the arterial or venous endothelial program (24). In numerous studies, EPHB4 and ephrin-B2 have been used as the endpoint markers for venous or arterial cells, respectively (24). Altered expressions of these genes have become accepted indicators of endothelial cell fate changes. The precise vascular functions for EPHB4 and ephrin-B2 have also been under intense investigation. Through several important studies, it has been established that the role of forward signaling through EPHB4 activation determines arteriovenous distinction, while reverse signaling through ephrin-B2 activation in the ligand cell appears to be required for later events during lymphangiogenesis (25–27). Despite these advances, how EPHB4 receptor phosphorylation mobilizes changes in intracellular communication to generate endothelial responses for the formation of arteries and veins remains elusive. Thus, we hypothesized that RASA1 plays a critical role downstream of this receptor to initiate a unique set of intracellular signals that promote arteriovenous differentiation. Participation of RASA1 in this EPHB4-driven process could provide the molecular rationale for how inactivating mutations in 1 allele of *RASA1* could cause CM-AVM. In dissecting RASA1's vascular function, our study has also revealed what we believe is a previously undefined role for endothelial mTORC1 overactivation in AVMs.

Results

Generating an animal model to study RASA1 deficiency. We note that genetic mouse models (11, 17), as well as retinal angiogenesis assays (ref. 28 and Supplemental Figure 1; supplemental material available online with this article; doi:10.1172/JCI67084DS1) have not been able to recapitulate the arteriovenous formation defects observed in CM-AVM lesions. Therefore, we generated zebrafish models to test our hypothesis that RASA1 functions as a critical effector for EPHB4 receptor signaling. The zebrafish is a versatile animal model that is particularly well suited for the analysis of vascular development. It permits real-time evaluation of abnormalities in blood vessel formation and function in a live organism. Its small size allows for oxygen diffusion to occur, so that embryonic development can proceed despite compromised cardiovascular function (29, 30). The ability to target specific genes with antisense morpholinos (MOs) also provides a rapid and efficient tool to induce gene knockdown in hundreds of animals (31). To facilitate functional analysis and visualization, we used transgenic lines for simultaneous imaging of blood vessel architecture and circulation in the same animal (Tg[*fli1:EGFP*]^{y1}:Tg[*gata1:dsRed*]) (32, 33).

We identified zebrafish homologues of *RASA1* (denoted *rasa1a* and *rasa1b*, respectively; Supplemental Figure 2A), each exhibiting a high level of conservation with the human RASA1 sequence. Since the zebrafish *rasa1* genes have not been described, we examined their expression patterns using in situ hybridization analysis (Supplemental Figure 2B). We found that both genes exhibited a ubiquitous, diffuse expression pattern from the 18-somite stage to 48 hours post fertilization (hpf), unlike the vascular-specific expression of the *VEGFR2* homologue *flk1* at the same stages (Supplemental Figure 2B). We proceeded with antisense MO targeting

of both genes, which also generated similar phenotypes (Figure 1). As in the *Rasa1*-null mouse (11), widespread cell death was observed throughout the head region, demonstrating conserved RASA1 function across vertebrate organisms (Figure 1, A–E). Interestingly, despite the lack of a vascular-specific expression pattern, distinct vascular defects were clearly seen and easily scored under reduced RASA1 function by 48 hpf. The most obvious problem was the lack of posterior blood flow to the caudal region of the body, as compared with control embryos, at the same stage (Figure 1, F–I). Since equivalent phenotypes were generated with either morphant, we focused our studies on the *rasa1a* morphant.

During normal vascular formation, the caudal vasculature beyond the yolk extension undergoes morphological changes over the first 5 days post fertilization (dpf) to eventually form a single caudal aorta and 1 caudal vein (34, 35). This begins with a caudal vascular plexus, which is formed by 48 hpf. At this stage, the majority of circulating blood flows through an upper caudal aorta and the ventral-most vein, while small interconnecting capillary-like channels also allow blood cells to pass through (Figure 1, F and G). Blood continuously flows through this region while it remodels into the caudal aorta and caudal cardinal vein by 5 dpf (34). In the *rasa1* morphant, however, the caudal vascular plexus did not form properly and an enlarged caudal vascular deformity was found instead (Figure 1, H and I). As a result, arterial blood flow was abruptly returned to the posterior cardinal vein, just anterior to this caudal vascular deformity (Figure 1I). The impediment to caudal blood flow is the most highly reproducible defect in this area; therefore, it was used to visually score hundreds of animals for functional caudal circulation (termed caudal functional assay; n = 100 embryos, N = 3 trials).

RASA1 functions downstream of EPHB4 in vivo. Since our hypothesis for CM-AVM places RASA1 as a critical endothelial effector downstream of EPHB4, we also examined the consequences of receptor knockdown. Remarkably, EPHB4 knockdown embryos faithfully mirrored the lack of caudal circulation and vascular deformities observed for the *rasa1* morphants (Figure 2, A–D, and Supplemental Figure 3, A–D), consistent with an in vivo interaction. In an early study, RASA1 was shown to bind the activated EPHB2 receptor through juxtamembrane phosphotyrosine (pY) motifs (pYIDPFTpYEDP; identical among 12 human Ephs, except for EphA1 and EphA10; ref. 20). The transient nature of the EPHB2-RASA1 interaction (20) suggested that an overexpression system is required to demonstrate a direct association for EPHB4 and RASA1. Therefore, we transfected HEK293T cells with both EPHB4 and RASA1 constructs to demonstrate that these 2 proteins can physically interact by coimmunoprecipitation (Figure 2E). To further investigate the functional relevance of an EPHB4-RASA1 recruitment in vivo, we designed 2 mutant receptors based on a previous report (36): EPHB4$_{FF}$, which removes 2 juxtamembrane RASA1 motifs (JM:**F**IDPFT**F**EDP, with boldface and underlines indicating mutated versions), and EPHB4$_{EE+Grb2}$, which removes 3 RASA1 potential sites and adds a GRB2-binding site to stimulate Ras (JM:**E**IDPFT**E**EDP). A third potential GRB2-binding site was added to the kinase domain: endogenous YTDK was changed to the GRB2 consensus sequence Y**VNV**. The WT and engineered EPHB4 receptor constructs were also validated through tyrosine phosphorylation and cell-surface expression (Figure 2, F and G).

Coinjection of the receptor MO with the WT *ephb4* mRNA effectively rescued caudal circulatory function and proper formation of
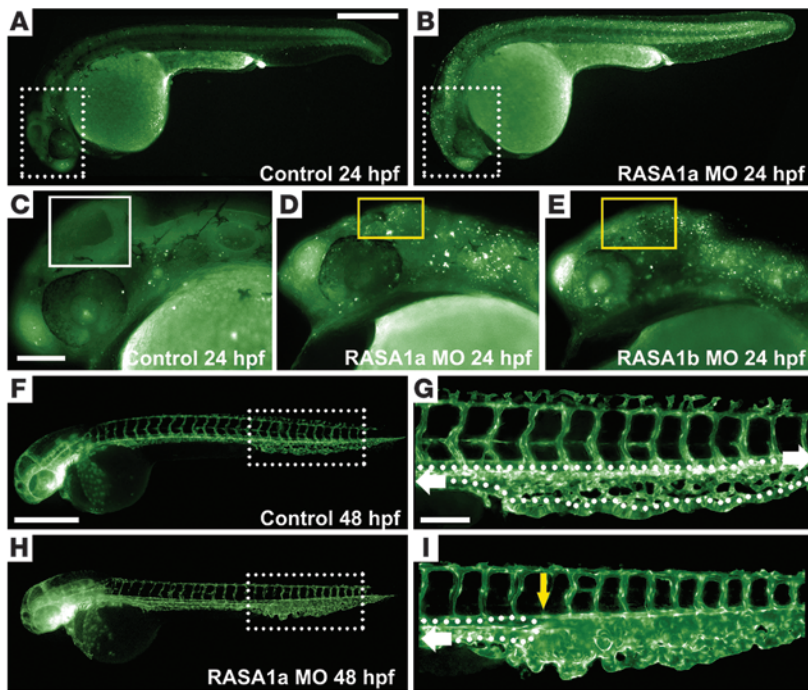
Figure 1
Reduced RASA1 function in zebrafish causes cell death and caudal vessel defect. (**A**–**E**) Acridine orange staining (cell death, particularly in the dotted boxed area) at 24 hpf on control (**A**) or *rasa1a* MO–injected (**B**) embryos. Higher magnification of hindbrain regions is boxed in white (control; **C**) or yellow (*rasa1a* MO and *rasa1b* MO; **D** and **E**). Similar hindbrain cell death was observed in *rasa1b* MO, as seen in *rasa1a* MO. (**F**–**I**) The *rasa1a* MO (750 μM) was injected in *Tg(fli1:egfp)*^{y1} to visualize endothelial cells at 48 hpf. Higher magnification of the caudal vessels of control (**F**) and *rasa1a* morphant (**H**) is shown in **G** and **I**, respectively. Dotted arrow indicates blood flow; yellow arrow indicates point of blood flow return. Scale bars: 500 μm (**A**, **B**, **F**, and **H**), 100 μm (**C**–**E**, **G**, and **I**).

the caudal vascular plexus. This resulted in a significant increase in the proportion of the embryos with normal blood flow and a decrease in those with severe phenotypes (Figure 2H and Supplemental Figure 4, A and B). Interestingly, receptor constructs lacking RASA1-binding sites, EPHB4$_{FF}$ and EPHB4$_{EE+Grb2}$, were unable to rescue the *ephb4* morphant (Figure 2H and Supplemental Figure 4, C–F). Taken together, these data strongly support an in vivo role for RASA1 recruitment to the activated EPHB4 receptor, where it promotes receptor signaling and mediates proper embryonic blood vessel formation.

Vascular consequences of EPHB4/RASA1 deficiency. In addition to the lack of caudal blood flow, we also observed a uniquely congruent intersegmental vessel (ISV) defect in both the *rasa1* and *ephb4* morphants, where more venous connections were made at the expense of arteries (Figure 3, A–D). During normal ISV formation, a venous endothelial cell sprouts from the cardinal vein at about 36 hpf. This endothelial cell may connect with a primary segment to form a vein, or it may not connect, in which case an artery is formed instead (Supplemental Figure 5A). In control embryos, a balanced ratio of arteries to veins are formed (37). Strikingly, under either RASA1 or EPHB4 deficiency, more secondary venous endothelial sprouts connect with the primary segments, resulting in a higher proportion of veins (Figure 3D and Supplemental Figure 5B). This arteriovenous endothelial cell connection defect and the caudal vessel deformity both reflect errors in embryonic blood vessel development, a presumed origin of human AVMs (2, 4). Thus, using the zebrafish model, we have captured some key features of CM-AVM, while demonstrating that RASA1 or EPHB4 can induce highly similar blood vessel abnormalities in vivo.

To gather further evidence that RASA1 functions as a critical mediator of endothelial EPHB4 receptor signaling, we designed synergistic experiments to include an ephrin-B2 ligand MO (Supplemental Figure 3E). For these experiments, each MO was used at subthreshold doses at which no phenotype is observed when injected alone (Figure 3, E–G). Since ephrin-B2 and EPHB4 form an endogenous ligand-receptor pair, their combined downregulation generated the largest caudal vessel defect (Figure 3H). We then coinjected the RASA1 MO with either the ligand or the receptor MO (Figure 3, I and J, respectively). Either of these combinations also demonstrated an enhancement of the caudal vascular defects, suggesting that RASA1 participates in endothelial ephrin-B2-EPHB4 signaling in vivo. Taken together with previous studies in which EPHB4 receptor forward signaling appears to drive embryonic angiogenesis (24–27), the consistent increase in the size of the caudal vessel region may be used as a simple readout for inadequate EPHB4 function.

Signaling pathway alterations in the enlarged caudal vessel. To investigate the cellular and molecular changes that result from diminished EPHB4 receptor function, we took advantage of the augmented caudal vessel generated by coinjection of the ephrin-B2 and *ephb4* MOs, designated double morphant (dMO), to provide a facile visual readout. We first determined whether this phenotype occurred as a result of increased cell proliferation by performing endothelial nuclei counts. Using a transgenic line where endothelial cells are labeled with a nuclearly localized EGFP, (*Tg(fli1:nEGFP)*^{y1}) (38), nuclei counts were obtained in a defined area bordered by 5 ISVs starting from the end of the yolk extension (Figure 4, A and B, *n* > 20 per condition; N = 3 experiments). We were surprised to find that there was no difference between control and dMO at 48 hpf (Figure 4C), suggesting that an increase in cell size may be responsible. If this is the case, then we might be able to observe changes in the TORC1 signaling pathway because overactivation of this pathway has been strongly linked to cell size enlargement (39). We performed experiments using an endothelial transgenic line in which red fluorescent protein expression is localized to the plasma membrane (40) in combination with a nuclearly targeted EGFP line (38). Although we were able to obtain visual confirmation of enlarged endothelial cell size, clear images were
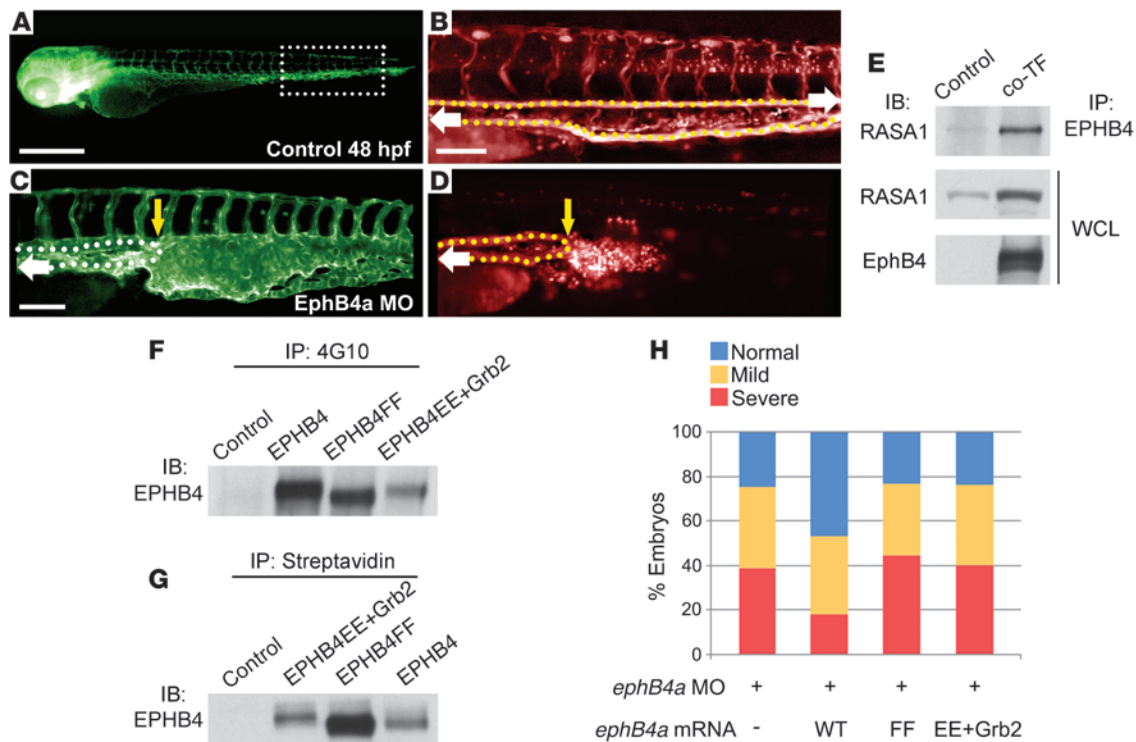
Figure 2
EPHB4 receptor rescue requires RASA1- binding motifs. The *ephb4a* MO (500 μM) was injected in double-transgenic line; refs. 32, 33), to visualize endothelial (green; **A** and **C**) and blood cells (red; **B** and **D**) in the same embryo at 48 hpf. (**A–D**) Caudal vessel phenotypes. (**B** and **D**) Blood flow in control (magnified boxed region in [**A**], or *ephb4a* morphant [**C**]). Yellow arrow indicates the end point of blood flow. Dotted arrows indicate direction of flow. Scale bars: 500 μm (**A**), 100 μm (**B–D**). (**E–G**) Expression of EPHB4 constructs and RASA1 in HEK293T cells. Control and EPHB4 construct–transfected cells were stimulated with clustered ephrin-B2–Fc (EfnB2a) (2 μg/ml). EPHB4 and RASA1 cotransfected (co-TF) cell lysates were immunoprecipitated (IP) using antibodies to EPHB4 or RASA1 (**E**, expression confirmed in whole cell lysate [WCL]). Receptor activation was determined by tyrosine phosphorylation using 4G10 antibody (**F**). EPHB4 construct–transfected cells were biotinylated and immunoprecipitated with streptavidin, followed by anti-EPHB4 blotting to determine cell-surface localization (**G**). (**H**) The *ephb4a* MO (500 μM) and *ephb4a* mRNA (30 ng/μl) coinjection phenotypes at 48 hpf (severe, mild, or normal) were converted to percentages. Caudal functional assay was used to score blood flow (*n* = 100 per condition).

difficult to obtain (data not shown). Therefore, we decided to examine signaling pathway phosphorylation levels using caudal tissues from large numbers of control and experimental animals.

We performed Western blot analysis using tissue lysates from the tail regions, which contained the caudal vascular abnormality. Among the phosphoproteins examined, the p-p70S6K signal was the strongest (Figure 4D), confirming a correlation between reduced EPHB4 signaling and TORC1 overactivation.

Drug rescue of EPHB4/RASA1-dependent vascular defects. In an independent approach to determining whether TORC1 signaling plays an important role in generating EPHB4-RASA1 vascular defects, we asked whether pretreatment of ephrin-B2/EPHB4/RASA1 pathway–deficient animals with PI3K and/or TORC1 inhibitory drugs could prevent or rescue blood vessel structure and/or function. Using 3 structurally distinct chemical inhibitors (GDC0941 targets PI3K, ref. 41; rapamycin targets TORC1, ref. 39; and BEZ235 targets both PI3K and TORC1, refs. 42, 43), formations of the dMO-induced large caudal vessel deformity were effectively prevented. Indeed, all 3 drugs were able to rescue the vascular defects and restore normal blood vessel structure and function to a majority of dMO-injected embryos (Supplemental Figure 6, A–F, and Supplemental Figure 7, A and B). Curiously, the ratio of inter-

segmental arteries to veins was also restored toward the normal, balanced proportion (Figure 4E), thus, providing evidence that these 2 phenotypes occurred as a result of PI3K-TORC1 overactivation. We also examined the ability of these compounds to rescue vascular abnormalities in RASA1-deficient embryos, as this gene is directly relevant to a human disease. In the presence of PI3K-TORC1 chemical inhibitors, normal blood vessel structure and function in the caudal vascular plexus and a balanced arteriovenous ratio were found in RASA1 (Figure 4F, Supplemental Figure 6, G–J, and Supplemental Figure 7, C and D), thus suggesting that full EPHB4 and RASA1 function are required to prevent overactivation of PI3K-TORC1 in the zebrafish model. Since RASA1 promotes RAS inactivation, it could affect both the RAS-PI3K-TORC1 and the RAS-ERK1/2 branches of intracellular signaling. Therefore, we also used a highly selective MEK1/2 inhibitor, CI-1040, in chemical rescue experiments. In contrast to the PI3K-TORC1 inhibitors, CI-1040 was unable to rescue the vascular defects in dMO or in RASA1 MO (data not shown). Together, these data provide evidence for an in vivo connection between reduced ephrin-B2–EPHB4–RASA1 expression and excessive PI3K/mTORC1 pathway activity as possible contributing factors in the formation of *RASA1*-dependent vascular lesions.
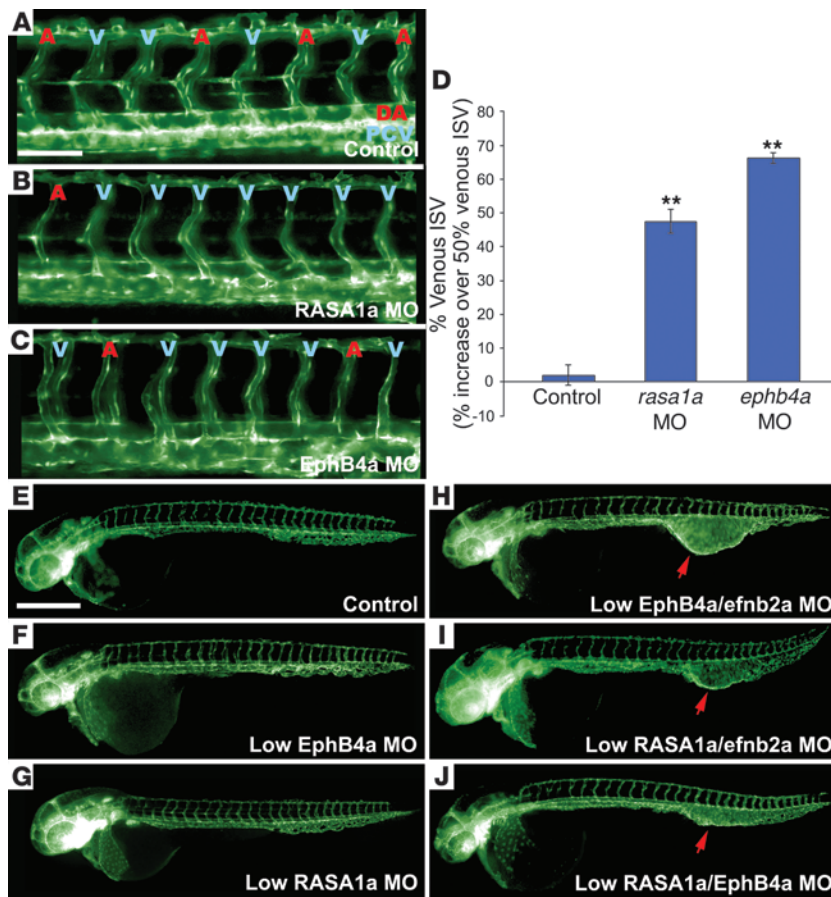
Figure 3
RASA1 participates in arteriovenous connections during vessel formation. (**A–D**) Arteriovenous connection assay was performed at 48 hpf. Balanced proportion of arterial (A, red) and venous (V, blue) ISVs in control embryo is shown (**A**). More venous ISVs were formed in *rasa1a* (750 μM; **B**) or *ephb4a* (500 μM, **C**) MO–injected embryos. Graph indicates the percentage increase in venous ISV over the balanced ratio (**D**; *n* = 20 per condition, mean ± SEM from 3 independent experiments; **P* < 0.01. DA, dorsal aorta; PCV, posterior cardinal vein. (**E–J**) Synergistic experiment was performed using subthreshold, low doses of MOs. Representative images of control (**E**) and embryos injected with low dose *ephb4a* (150 μM; **F**) or *rasa1a* (250 μM; **G**) MO show no phenotype. Augmented caudal vascular defects with coinjection of low-dose *ephb4a*, *rasa1a*, or *efnb2a* (250 μM) MO are also shown (**H–J**). Red arrows indicate enlarged caudal vessels. Scale bars: 100 μm (**A–C**); 500 μm (**E–J**).

Endothelial mTORC1 activation enhances EPHB4/RASA1 deficiency. To establish that an increase in endothelial TORC1 pathway activity is linked to the vascular defects observed in the *ephb4* or *rasa1* morphants, we designed a transgenic zebrafish line to have increased blood vessel TORC1 activity. Since mTOR is a very large kinase, overexpression of this kinase is a difficult task. Therefore, we employed a strategy to enhance TORC1 activity through targeting its regulator, RHEB. RHEB is a small GTPase known to stimulate mTORC1 activity in its GTP-bound state (39). In the mammalian system, structural work has demonstrated that a constitutively activated RHEB mutant construct, RHEBS16H (44, 45), can render this small GTPase resistant to the activity of its GAP, TSC1/2.

An alignment of the human and zebrafish RHEB sequences demonstrated complete identity in this region; therefore, generation of a similar construct was likely to overactive the TORC1
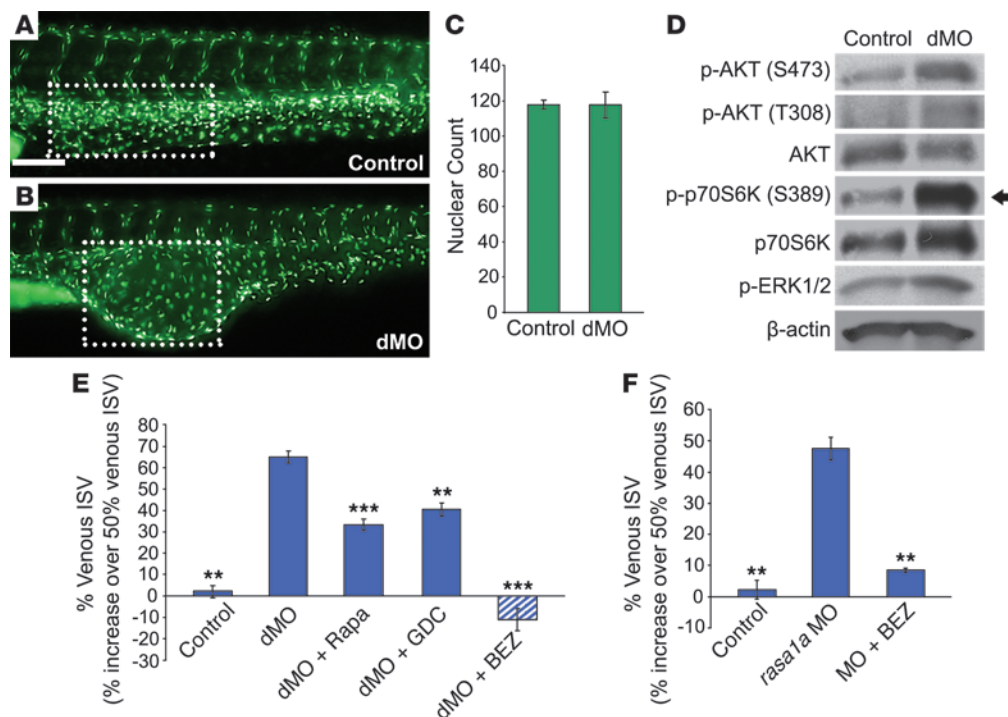
kinase. Using the zebrafish RhebS16H construct, we performed mRNA overexpression analysis as a functional test. We found that embryos injected with the zebrafish *RhebS16H* mRNA also featured an abundance of venous ISVs (Supplemental Figure 8A) analogous to the *ephb4* and *rasa1* morphants and in agreement with our observations of TORC1 overactivity. Furthermore, this arteriovenous defect was prevented by rapamycin treatment (Supplemental Figure 8B).

To create a transgenic zebrafish line overactivating TORC1, we placed the zebrafish RhebS16H construct under the endothelial *fli1* promoter (Supplemental Figure 8, C–G, and ref. 32). To facilitate transgenesis, we used the Tol2 transposon–mediated transgenesis method (46–49). Our transgene was designed to include a fluorescent reporter driven by the *cmlc* promoter (Supplemental Figure 8E and ref. 49), so that cardiac expression of EGFP enabled the visual selection of embryos with incorporation of the transgene. In this process, F_0 embryos with a normal appearance and fluorescent hearts were selected to be raised as potential founders. After 3 months, when F_0 founders reached sexual maturity, they were outcrossed with the $Tg(fli1:EGFP)^{y1}$ (32) line to produce embryos for an F_1 generation. Since endothelial cells are labeled by EGFP in this line, blood vessel defects can be visually monitored while expression of EGFP in the myocardium suggested incorporation of the transgene. These embryos were selected and raised for the F_2 generation. In a similar fashion, characterization of F_3 embryos derived from the F_2 incrosses revealed that WT siblings exhibited no obvious vascular defects (Supplemental Figure 8, C and D). Genomic incorporation and transgene expression were confirmed by PCR, RT-PCR, and sequence analysis using individual embryos from each line as compared with WT sibling controls (data not shown). Experiments in this study used F_3 and F_4 generations of the $Tg(fli1:RhebS16H)$ transgenic line.

To examine whether enhanced endothelial TORC1 activity is sufficient to synergize with the vascular phenotype observed in *rasa1* and *ephb4* morphant, we employed subthreshold doses of the *rasa1* MO, the *ephb4* MO, or dMO in either WT siblings or *RhebS16H* transgenic embryos. In each case, the subthreshold MO doses did not disrupt caudal vascular function in WT siblings (Figure 5, A–C). However, in the *RhebS16H* transgenic background, $Tg(fli1:RhebS16H):Tg(fli1:EGFP)^{y1}$, enlargement of caudal vessel and a lack of posterior blood flow occurred with *rasa1* MO (Figure 5D), *ephb4* MO (Figure 5E), or dMO (Figure 5F) injections. Therefore, these results independently support the hypothesis that endothelial TORC1 overactivation underlies the vascular defects observed in *ephb4* and *rasa1* morphants.

Elevated mTORC1 signaling in human AVM. To investigate whether this endothelial signaling axis from EPHB4 to RASA1 to mTORC1 identified in the zebrafish model is relevant to human AVMs, we
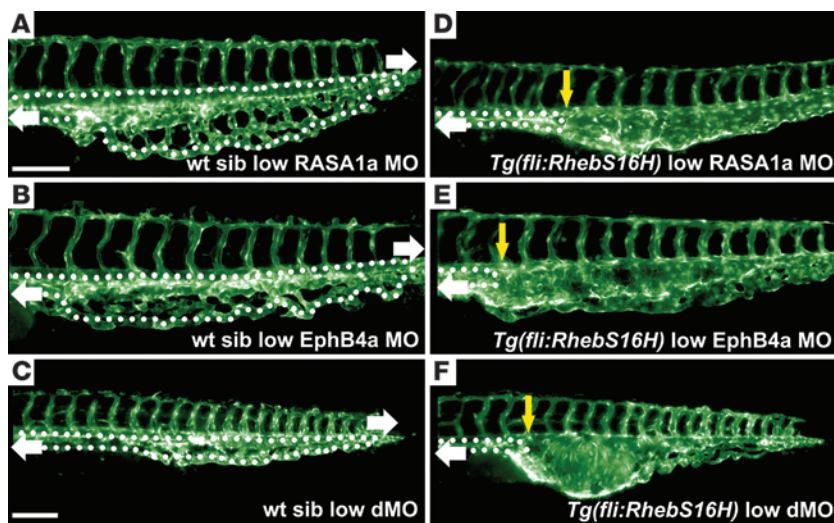
Figure 4
Overactive TORC1 contributes to vascular phenotypes. (**A** and **B**) Endothelial nuclei counts were done in the boxed area spanning 5 ISVs caudally from the end of yolk extension in control embryo (**A**) or embryo coinjected with *ephb4* and *efnb2a* MOs (dMO; both MO at 250 μM; **B**), at 48 hpf using an endothelial line with nuclearly targeted EGFP (38). Scale bar: 100 μm (**A** and **B**). (**C**) Graph showing the result of nuclei count (*n* > 20 per condition; mean ± SEM from 3 independent experiments). (**D**) Western blot showing embryonic tail lysates from control or dMO, detected with antibodies as indicated. Black arrow indicates overactive TORC1 pathway in dMO lysates. (**E** and **F**) Chemical rescue of dMO (**E**) or *rasa1*a morphant (**F**) using the arteriovenous connection assay. Inhibitors used are as follows: rapamycin (rapa) (400 nM), GDC0941 (GDC) (250 nM), or BEZ235 (BEZ) (250 nM). *n* = 20 per condition; mean ± SEM from 3 independent experiments; **$P < 0.01$, ***$P < 0.001$. See also Supplemental Figures 6 and 7.

tested surgically resected patient samples to include both *RASA1* mutation–positive and phenotypically similar AVMs. Tissues from 11 patients with various vascular anomalies were tested: 3 CM-AVM (OMIM 608354, 5q13.3) samples with confirmed *RASA1* mutations; 2 samples from Parkes Weber syndrome (PWS) (OMIM 608355, 5q13.3), which is associated with *RASA1* mutations (5, 6); and 6 other AVMs. For control blood vessel staining, we used subcutaneous tissue from a healthy individual. We tested for phospho-S6 (p-S6) as an indicator of mTORC1 pathway activation and phospho-ERK1/2 (p-ERK1/2), as a marker for RASs-ERK1/2 activation. Little or no staining was detected for p-S6 or p-ERK1/2 in normal vessels (Figure 6A). However, tissues from the patients with confirmed *RASA1* mutations showed staining for p-S6, particularly in endothelial cells lining the vessel lumen as well as surrounding cells (Figure 6, B–G). In PWS (Supplemental Figure 9, A and B), both p-S6 and p-ERK1/2 stained positive in blood vessels. For all the other AVMs, a strong endothelial p-S6 signal was clearly seen, but the p-ERK1/2 signal was indistinguishable from the background (Supplemental Figure 9, C–E, and data not shown). In this set of patient samples, we demonstrate a consistent increase in mTORC1 signaling in 11 out of 11 samples of human AVMs. For the RAS-ERK1/2 pathway, p-ERK1/2 staining was elevated in 5 out of 11 (45%) of the samples tested. Thus, mTORC1 overactivation appears to be an important and persistent molecular driver for AVMs, including *RASA1*-dependent CM-AVMs.

Discussion

The prominence of RAS oncoproteins in human cancers has provided a strong driving force to determine its cellular function and to define its molecular partners (50). Discovering that RASGAPs, such as RASA1, function as negative regulators of RAS has improved our understanding of how certain oncogenic mutations allow RAS to avoid RASGAPs and remain constitutively activated (51, 52). Activated RAS binds to and activates the serine-threonine kinase RAF as a major effector. RAF then phosphorylates the MEK1/2 kinases, which in turn activate ERK/MAPK by phosphorylation at both tyrosine and threonine residues (53). Furthermore, RAS can also stimulate PI3K through direct interaction with the catalytic p110α subunit (54–57). Despite biochemical and cancer studies confirming these intracellular interactions with RAS, it remains unknown how these pathways are utilized to generate specific cellular responses in vivo. Thus, determining how autosomal dominant mutations in the globally expressed *RASA1* gene induce vascular-specific lesions can provide an important entry point to understanding the in vivo regulation of RAS downstream pathways that may be applicable to many human diseases including cancer.

One of the difficulties in studying vascular lesions is the lack of an accessible animal model. By employing the zebrafish as an alternative vertebrate model, we demonstrated that reduced RASA1 function leads to impaired circulation and arteriovenous miscon-

Figure 5
Enhanced RASA1 or EPHB4 knockdown phenotypes in a transgenic line with endothelial TORC1 activation. (**A–F**) Low, subthreshold dose of either *rasa1a* MO (250 μM; **A** and **D**), *ephb4a* MO (150 μM; **B** and **E**), or dMO (150 μM each; **C** and **F**) was injected in WT sibling or *Tg(fli1:RhebS16H)* embryos. At 48 hpf, WT sibling with low-dose MO injected had no vascular phenotype (**A–C**); however, when injected in embryos with *RhebS16H* transgene, the vascular phenotypes were augmented (**D–F**). Experiments for this paper were conducted using F_3 and F_4 embryos. Scale bars: 100 μm.
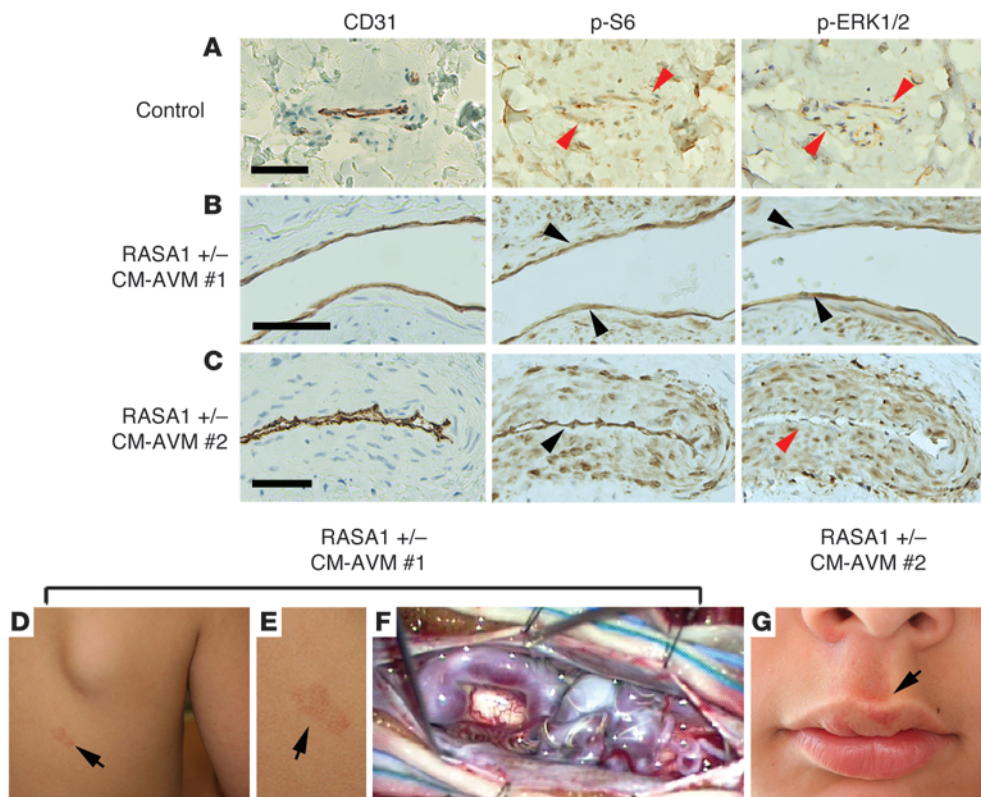
nections in hundreds of experimental animals. Furthermore, we also demonstrated that these RASA1-dependent vascular defects are linked to its role as an endothelial effector for the EPHB4 receptor. Since EPHB4 is known to promote endothelial cell segregation in the formation of the aorta and cardinal vein (58, 59), we suggest that reduced RASA1 function compromises the ability of the EPHB4 receptor to execute its full function, leading to abnormalities in the formation of arteries and veins. By investigating the molecular nature of reducing ephrin-B2 and EPHB4 function in our animal model, we uncovered an unexpected increase in endothelial mTORC1 activity. To directly interrogate this relationship, we created a transgenic zebrafish line that overactivates TORC1 in endothelial cells. Using this line, we observed enhanced vascular defects using low, subthreshold levels of *rasa1*, *ephb4*, or ephrin-B2/*ephb4* MOs. Collectively, these data strongly support a functional connection between EPHB4, RASA1 and mTORC1.

Ultimately, a signaling pathway defined in any animal model can only provide strong insights into human disease if it can be rigorously tested and the knowledge is clinically relevant. In our study, we tested our pathway connection between EPHB4, RASA1, and mTORC1 using multiple methods. However, the most convincing data in our study have been the robust chemical rescues. Pretreatment of EPHB4/RASA1 knockdown animals with preclinical PI3K and/or mTORC1 drugs dramatically restored blood vessel circulation and normal architecture in affected animals. Taken together, these data suggest a strong likelihood that perturbed EPHB4-RASA1-mTORC1 signaling also underlies the vascular defects in human CM-AVM. In a normal human blood vessel sample, the activity level of the mTORC1 and ERK is low, as indicated by diffused staining for both pERK and pS6 markers. However, in AVM samples, staining for pERK and pS6 is often very high, and much of the staining is localized to endothelial cells lining the blood vessel wall. In 11 samples of AVMs, the pERK signal was elevated in 45% while pS6, indicating mTORC1 activity, was increased in 100% of patient samples, demonstrating that results gleaned from the zebrafish model can be applied to investigating the fundamental signaling pathway changes in patient samples.

In an effort to define an endothelial role for *RASA1* as the causative gene in CM-AVM, we propose a model where an endothelial signaling axis stemming from the activated EPHB4

receptor leads to the recruitment of RASA1. RASA1 stimulates RAS inactivation, resulting in the silencing of its downstream components. These signaling changes reduce endothelial mTORC1 activity (Supplemental Figure 10A). We envision that EPHB4 recruitment of RASA1 generates a prolonged effect on RAS inactivation. Unlike other RTKs, EPH family receptors require high-order oligomerization to be fully stimulated (60); therefore, large numbers of clustered EPHB4 receptors could provide numerous binding sites for RASA1 molecules to sustain RAS inactivation (Supplemental Figure 10A). However, under conditions of partial RASA1 function, as could be the case for CM-AVM, insufficient RAS inactivation could disrupt the process of arteriovenous differentiation, creating malformations in capillaries, arteries, and veins (Supplemental Figure 10B). This model is supported by our data using the zebrafish model and patient AVM samples. It is also consistent with previous in vivo studies on EPHB4 receptor function (21–23), and provides a molecular explanation for the causative role of *RASA1* mutations in CM-AVM. Our model suggests that this genetic deficiency would also provide the driving force behind the recurrence of AVMs after intervention (10) because CM-AVM patients would likely have inadequate RASA1 function when new vessels are being formed during the process of recovery.

Since the original identification of a role for EPHB4 in arteriovenous differentiation (21–23), endogenous endothelial effectors have not been reported. Here, we provide a molecular connection from EPHB4 to RASA1 to mTORC1 as key players that participate in the differentiation of arteries and veins. A number of rapamycin-like drugs (rapalogues) have been developed for cancer treatment. We note that these inhibitors may also be useful for the treatment of AVMs. From our animal model studies, it seems feasible that counteracting mTORC1 overactivation may be sufficient to encourage normal blood vessel formation, despite a predisposition for reduced RASA1 function. Since human AVMs also exhibit the same characteristic increase in mTORC1 activity, it may be possible to use rapalogues for a short period of time following sclerotherapy, embolization, and/or surgical removal of AVMs to promote normal neovascularization in the affected area. The use of mTORC1 inhibitors in this manner may reduce the tendency for AVMs to recur.

Figure 6
Overactive endothelial mTORC1 is consistently found in *RASA1* mutation–positive patient tissues. Representative images of immunostaining with CD31 (PECAM-1, marker for endothelial cells), p-S6 (S235/236; marker for mTORC1 activation) or p-ERK1/2 (marker for increased RAF-MEK activation) from healthy tissue (**A**) or resected CM-AVMs from patients with *RASA1* mutation (**B** and **C**). Black arrowheads indicate positive endothelial staining (overlapped staining with CD31); red arrowheads indicate no endothelial staining. (**D–F**) CM-AVM patient no. 1 (CM-AVM no. 1; **B**) had capillary stain on the back (**D**, enlarged in **E**) overlying a spinal cord AVM (**F**, sutures holding back open dura mater exposing AVM on spinal cord; photo, courtesy of Edward Smith, Boston Children's Hospital). (**G**) CM-AVM patient no. 2 (CM-AVM no. 2; **C**) had CM-AVM on the lip. Scale bars: 50 μm (**A–C**).

Evidence for an effective use of mTORC1 inhibitors has been provided through treatment of children with a TSC-dependent type of brain tumor (61). Furthermore, in a retrospective study on patients with clinically severe forms of vascular anomalies, treatment with rapamycin was shown to improve symptoms for 6 out of 6 patients (62). Our study supports the inclusion of CM-AVM and/or PWS in clinical trials. The ability to use an FDA-approved drug for the treatment of additional human diseases provides significant savings of the time and resources needed to develop new drugs. A targeted therapy for a vascular anomaly would also contribute to the goal of developing "personalized medicine" for patients and their family members living with genetic mutations in the *RASA1* gene.

Methods

Materials. Antibodies used in this study were acquired as follows: anti–phospho-AKT (Ser473), phospho-AKT (Thr308), phospho-p70S6K (Thr389), phospho-ERK1/2 (p44/42), AKT, p70S6K, and ERK1/2 antibodies (Cell Signaling Technology); anti-EPHB4 and anti-actin antibodies (Sigma-Aldrich); anti-p120-RasGAP (Santa Cruz Biotechnology Inc.), anti-human IgG Fc fragment specific antibody (Jackson Immunoresearch Laboratories); anti-EPHB4 antibody (R&D Systems); and G10 anti-pY antibody (gift from Thomas M. Roberts, Department of Cancer Biology,

Dana-Farber Cancer Institute, Boston, Massachusetts, USA). For immunohistochemistry, monoclonal anti-phospho-AKT (S473), phospho-S6 (S235/236) and phospho-ERK1/2 from Cell Signaling Technology were used. Rapamycin was from Enzo Life Sciences International; GDC0941 and BEZ235 were from Axon Medchem BV.

Mouse retinal angiogenesis assay. Protocol for this assay has been published elsewhere (63, 64). Briefly, gene knockdown in mouse retina was performed by injecting RASA1 siRNA (0.5 μg; Supplemental Table 1) intravitreally into the left eye of C57BL/6 mouse at P6. Mouse RASA1 siRNA was designed as previously described (65). The same amount of control siRNA (Ambion) was injected into the right eye of the same mouse to serve as a control.

Retinal vascular formation was assessed 2 days after injection using flat-mounted, fluorescein-conjugated isolectin staining and immunohistochemical analysis ($n > 5$). Quantification of vessel density was performed using Adobe Photoshop as described previously (63, 64). Retinal RNA was purified and *RASA1* expression was quantified using quantitative RT-PCR (qRT-PCR). Primers used for this analysis are also shown in Supplemental Table 2.

Cell culture. Human embryonic kidney (HEK) 293T cells were cultured in DMEM medium containing 10% FBS at 37°C, 5% CO_2, for all experiments. Cells were harvested following stimulation with clustered ephrin-B2-FC for 30 minutes. Recombinant ephrin-B2-Fc chimera (R&D Systems) was

preclustered as previously described (66). Briefly, recombinant ephrin-B2-Fc chimera was incubated with anti-human IgG Fc fragment–specific antibody (Jackson Immunoresearch Laboratories) for 1 hour on a rocker at 4°C. Clustered ephrin-B2-Fc was dissolved in medium to a final concentration of 1 to 2 μg/ml for stimulation.

DNA constructs, mutagenesis, and transfection. Human full-length *RASA1* cDNA clone for transfection was purchased from OriGene Technologies. The zebrafish *ephb4a* cDNA sequence was used to generate the *ephb4a* MOs as well as the full-length *ephb4a* mRNAs (WT and mutants). WT or mutant *ephb4a* or *rheb* cDNAs were subcloned into pCS2+ vector. Mutagenesis of EPHB4a (EPHB4a$_{FF}$, EPHB4a$_{EE+Grb2}$) and RHEB (RHEBS16H) was performed using the QuikChange XL Site-Directed Mutagenesis Kit (Stratagene) and confirmed by DNA sequencing.

Biotinylation of cell surface proteins. Cells were washed with PBS twice and incubated with biotinylation buffer (0.1 mg/ml Sulfo-NHS-SS-Biotin [Thermo Fisher Scientific], 50 nM NaPO$_4$ [pH 8.0-8.5], 110 mM NaCl) for 30 minutes on ice. Cells were then washed 3 times with PBS and lysed with RIPA buffer supplemented with protease inhibitors and sodium orthovanadate.

Immunoprecipitation and coimmunoprecipitation. For immunoprecipitation, cells were lysed in RIPA lysis buffer supplemented with protease inhibitors and sodium orthovanadate, and 250 μg of lysate was incubated with EPHB4 antibody (R&D Systems) or 4G10 antibody for 1 hour. For coimmunoprecipitation, cells were lysed in HNTG buffer (20 mM HEPES [pH 7.5], 150 mM NaCl, 0.1% Triton-X 100, 10% glycerol) supplemented with protease inhibitors and sodium orthovanadate, and 2 mg of lysate was used for the incubation with the primary antibody. Then, protein A/G PLUS-Agarose was added (Santa Cruz Biotechnology Inc.) for incubation overnight at 4°C on a rocker. For biotinylated cells, 250 μg of lysate was incubated with streptavidin beads (Thermo Fisher Scientific) for 2 hours. Beads were washed 3 times with PBS or lysis buffer used to lyse the cells, and bound proteins were resolved on SDS-PAGE, then transferred onto nitrocellulose.

Human tissue section and immunohistochemistry. Patients having undergone surgical excision of *RASA1* mutation–positive or related lesions were identified via review of medical records at the Vascular Anomalies Center, Boston Children's Hospital. Six formalin-fixed, paraffin-embedded patient tissue sections, 3 with confirmed *RASA1* mutations (de Duve Institute, Université Catholique de Louvain, Brussels, Belgium), were obtained (IRB S11-02-0031). Detection of phosphoproteins, p-S6 and p-ERK1/2, was validated by immunohistochemistry. The p-S6 (S235/236) rabbit monoclonal antibody was used at a 1:200 dilution after antigen retrieval with 10 mM sodium citrate steam treatment for 20 minutes (as previously described) (67). The p-ERK1/2 rabbit monoclonal antibody was used at a 1:100 dilution, also after sodium citrate antigen retrieval. Secondary biotinylated anti-rabbit IgG (Vector Labs) was used at a 1:1000 dilution, and tertiary streptavidin–horseradish peroxidase (Vector Labs) was used. The CD31 antibody staining was performed by the Dana-Farber/Harvard Cancer Center Specialized Histopathology Core. Sections were blinded to the researcher during staining and processing.

Maintenance of zebrafish. Breeding zebrafish were normally maintained at 28.5°C on a 14-hour light/10-hour dark cycle in a recirculating tank system. The following lines were used in this study: WT AB line; Tg(fli1:egfp)^{y1}; Tg(gata1:dsRed); Tg(fli:nEGFP)^{y7} (32, 33, 38). Embryos were collected by natural spawning, and raised in E3 embryo buffer (5 mM NaCl, 0.17 mM KCl, 0.33 mM CaCl$_2$, 0.33 mM MgSO$_4$) at 28.5°C.

Microinjection. Zebrafish *ephb4a* cDNA was linearized, and capped RNAs were in vitro transcribed using the Message Machine Kit (Ambion Inc.) following the manufacturer's instructions. Two nanoliters of each MO or mRNA were microinjected into 1-cell stage embryos using a gas-driven microinjector (Medical Systems Corp.). All mRNAs were injected at 30 ng/μl. Sequences for each MO are presented in Supplemental Table 3.

RNA in situ hybridization. Whole-mount zebrafish in situ hybridization using digoxigenin-labeled sense and antisense RNA probes was performed using standard methods, as previously described (68). RNA probes containing digoxigenin-11-UTP (Roche Applied Science) were visualized using the BM purple alkaline phosphatase substrate (Roche Applied Science).

Zebrafish phenotype scoring. We employed 2 types of assays to score 2 distinct vascular phenotypes in morphants. To evaluate caudal blood vessel function, we used a caudal functional assay (*n* = 100 embryos per condition; N = 3 for all experiments). Phenotypes were categorized into either normal (indistinguishable from WT controls) or limited blood flow (including mild [partial blood flow] or severe [no blood flow]) at 48 or 72 hpf. The change in proportion of normal embryos under each condition was compared with the untreated morpholino-injected embryos to determine rescue efficiency. To quantitate the arteriovenous ISV connection, we designed the "arteriovenous connection assay" (*n* = 20 embryos per condition; N = 3, for all experiments). A counting region containing 8 ISVs (from mid-trunk to end of yolk extension) was used for each embryo at 48 hpf. Normalized against a ratio of 50% venous ISVs (and 50% arterial ISVs), a relative percentage change in venous ISVs was used in quantitation and analysis. Both assays were performed using double-transgenic embryos; refs. 32, 33), with endothelial and red blood cells labeled in green and red, respectively. An endothelial line with nuclearly targeted EGFP (38) was used to determine cell number in the area spanning 5 caudal ISVs starting from the end of yolk extension at 48 hpf (*n* > 20 embryos per condition; N = 3). Student's *t* test was used for all statistical analysis, and all data are shown as means ± SEM from 3 independent experiments.

Validation of MO knockdown efficiency. MOs were designed to inhibit splicing of pre-mRNA or to block the translational start site. Knockdown efficiency for *ephb4a* splice MO was confirmed by RT-PCR (Supplemental Table 4 for primers). For *ephb4a* and ephrin-B2a AUG MOs, the TNT T7 Quick for PCR DNA and Transcend Non-Radioactive Translation Detection Systems (Promega) were used according to the manufacturer's instructions. Forward primers were designed, including T7 promoter sequence, Kozak sequence, AUG start codon followed by *ephb4a* or ephrin-B2a coding sequence; reverse primers were designed, including EphB4a or ephrin-B2a sequence followed by stop codon and poly-A tail. Two different forward primers were designed for *ephb4a* or ephrin-B2a. For *ephb4a*, these included the following: (a) a primer including an *ephb4a* MO target 5′ UTR sequence, and (b) a primer lacking a target 5′ UTR sequence. For ephrin-B2a, these included the following: (a) a primer with WT ephrin-B2a sequence with the MO targeting site; (b) a primer with silent mutations at the MO targeting site. Mutations were induced using QuikChange XL Site-Directed Mutagenesis Kit (Stratagene). Together with the reverse primers, PCR was performed using full-length *ephb4a* or ephrin-B2a construct as a template. The resulting PCR products were used in reactions containing biotin-lysysl-tRNA, with or without MO targeting *ephb4a* or ephrin-B2a. as described by the manufacturer. Protein samples were then separated on SDS-PAGE, followed by a standard Western blot protocol. Membranes were probed with streptavidin-HRP, and proteins were detected by chemiluminescence. Zebrafish RASA1a (*rasa1*, XM_001341973, 82% amino acid identity) and RASA1b (similar to p120G*AP*, XM_001921687, 76% amino acid identity) sequences were identified through bioinformatic analysis. Using these sequences, both *rasa1* MOs were designed against an intron-exon boundary (i2e3). Targeting of each transcript was confirmed by RT-PCR (Supplemental Table 4 for primers).

Acridine orange staining. Dechorionated embryos were placed in 50 μg/ml acridine orange (acridinium chloride hemi-[zinc chloride]; Sigma-Aldrich) diluted in 10% Hank's saline solution for 30 minutes at room temperature in the dark. Embryos were then washed 3 times for 10 minutes with 10% Hank's saline solution and were mounted on glass slides for fluorescence microscopy.

Zebrafish tail lysate preparation. Zebrafish embryonic tails (beyond yolk extension, n = 300) were carefully microdissected using a scalpel and collected into a microfuge tube on ice, then homogenized in RIPA lysis buffer, supplemented with protease inhibitors and vanadate. Western blot analysis was performed using 100 μg of control or experimental lysate.

Chemical inhibitor treatments. Rapamycin (400 nM), GDC0941 (250 nM), or BEZ235 stocks (250 nM) were dissolved in DMSO, then diluted in E3 embryo buffer. Zebrafish embryos at 24 hpf were treated with each inhibitor at 28.5°C as previously described (69) for 48 hours. Rapamycin was refreshed every 24 hours.

Zebrafish transgenesis. Transgenesis constructs were generated using Multisite Gateway system (Invitrogen) and the Tol2kit system (49). Briefly, gain-of-function zebrafish Rheb mutant RhebS16H cDNA was cloned into the pME-MCS vector. An LR clonase reaction was used to recombine the p5E-*fli1* 5′ entry clone, the pME-RhebS16H middle entry clone, and the p3E-polyA 3′ entry clone into the pDestTol2CG2 vector. This recombination resulted in the generation of the pDestTol2CG2-fli1:RhebS16H vector.

Zebrafish embryos were injected with 2 nl of 25 ng/μl (50 pg) pDestTol-2CG2-fli:RhebS16H and 35 ng/μl (70 pg) Tol2 transposon mRNA within 15 minutes of fertilization. Injected embryos were raised to 48 hpf, and those with both cardiac myosin light chain promoter-driven (cmlc2) EGFP expression and with WT appearance were raised as potential founders (F_0). Once reaching sexual maturity, these founders were outcrossed to the *Tg(fli1:EGFP)^{y1}* line (32) to visualize endothelial cells. Embryos that lacked the cardiac fluorescent reporter were the WT siblings, with no obvious defects. This process continued in the selection of F_2, F_3, and F_4 generations to generate the *Tg(fli1:RhebS16H)* line.

Statistics. A 1-tailed Student's t test was used for most statistical analyses, with the exception of Figure 4, E and F, where a 2-tailed Student's t test was used. Data are shown as mean ± SEM from 3 independent experiments (n = 3). The sample sizes are indicated with "n". In each case, the P value is also provided. $P < 0.05$ was considered significant.

Study approval. All animal protocols were approved by the Institutional Animal Care and Use Committee of Boston Children's Hospital, protocol number 13-04-2383R. The use of paraffin blocks containing patient tissue samples were approved by the IRB, protocol M09030158; related lesions were identified via review of medical records at the Vascular Anomalies Center, also approved by the IRB, protocol M09030158, at the Boston Children's Hospital. Three formalin-fixed, paraffin-embedded patient tissue sections with confirmed *RASA1* mutations were obtained from the de Duve Institute under IRB protocol S11-02-0031. Informed consent was obtained from participants or their guardians prior to tissue donation.

Address correspondence to: Joanne Chan, Department of Biological Sciences and Minority Men's Health Initiative, 100 E. Queen Street, Hampton University, Hampton, Virginia, USA. Phone: 757.728.6030; Fax: 757.728.6051; E-mail: joanne.chan@hamptonu.edu.

John D. Mably and Joanne Chan's present address is: Department of Biological Sciences and Men's Health Initiative, Hampton University, Hampton, Virginia, USA.

1. Marler JJ, et al. Successful antiangiogenic therapy of giant cell angioblastoma with interferon alfa 2b: report of 2 cases. *Pediatrics*. 2002;109(2):E37.
2. Mulliken JB, Glowacki J. Hemangiomas and vascular malformations in infants and children: a classification based on endothelial characteristics. *Plast Reconstr Surg*. 1982;69(3):412–422.
3. Boon LM, Ballieux F, Vikkula M. Pathogenesis of vascular anomalies. *Clin Plast Surg*. 2011;38(1):7–19.
4. Greene AK. Vascular anomalies: current overview of the field. *Clin Plast Surg*. 2011;38(1):1–5.
5. Eerola I, et al. Capillary malformation-arteriovenous malformation, a new clinical and genetic disorder caused by RASA1 mutations. *Am J Hum Genet*. 2003;73(6):1240–1249.
6. Boon LM, Mulliken JB, Vikkula M. RASA1: variable phenotype with capillary and arteriovenous malformations. *Curr Opin Genet Dev*. 2005;15(3):265–269.
7. Revencu N, et al. Parkes Weber syndrome, vein of Galen aneurysmal malformation, and other fast-flow vascular anomalies are caused by RASA1 mutations. *Hum Mutat*. 2008;29(7):959–965.
8. de Wijn RS, Oduber CE, Breugem CC, Alders M, Hennekam RC, van der Horst CM. Phenotypic variability in a family with capillary malformations caused by a mutation in the RASA1 gene. *Eur J Med Genet*. 2012;55(3):191–195.
9. Revencu N, et al. RASA1 Mutations and Associated Phenotypes in 68 Families with Capillary Malformation-Arteriovenous Malformation. *Hum Mutat*. 2013;34(12):1632–1641.
10. Liu AS, Mulliken JB, Zurakowski D, Fishman SJ, Greene AK. Extracranial arteriovenous malformations: natural progression and recurrence after treatment. *Plast Reconstr Surg*. 2010;125(4):1185–1194.
11. Henkemeyer M, et al. Vascular system defects and neuronal apoptosis in mice lacking ras GTPase-activating protein. *Nature*. 1995;377(6551):695–701.
12. Brouillard P, Vikkula M. Genetic causes of vascular malformations. *Hum Mol Genet*. 2007;16(spec no. 2):R140–R149.
13. Bernards A. GAPs galore! A survey of putative Ras superfamily GTPase activating proteins in man and Drosophila. *Biochim Biophys Acta*. 2003;1603(2):47–82.
14. Downward J. Targeting RAS signalling pathways in cancer therapy. *Nat Rev Cancer*. 2003;3(1):11–22.
15. Friedman E, Gejman PV, Martin GA, McCormick F. Nonsense mutations in the C-terminal SH2 region of the GTPase activating protein (GAP) gene in human tumours. *Nat Genet*. 1993;5(3):242–247.
16. Mitsudomi T, Friedman E, Gejman PV, McCormick F, Gazdar AF. Genetic analysis of the catalytic domain of the GAP gene in human lung cancer cell lines. *Hum Genet*. 1994;93(1):27–31.
17. Lapinski PE, et al. RASA1 maintains the lymphatic vasculature in a quiescent functional state in mice. *J Clin Invest*. 2012;122(2):733–747.
18. Margolis B, et al. The tyrosine phosphorylated carboxyterminus of the EGF receptor is a binding site for GAP and PLC-γ. *EMBO J*. 1990;9(13):4375–4380.
19. Kaplan DR, Morrison DK, Wong G, McCormick F, Williams LT. PDGF β-receptor stimulates tyrosine phosphorylation of GAP and association of GAP with a signaling complex. *Cell*. 1990;61(1):125–133.

20. Holland SJ, et al. Juxtamembrane tyrosine residues couple the Eph family receptor EphB2/Nuk to specific SH2 domain proteins in neuronal cells. *EMBO J.* 1997;16(13):3877–3888.

21. Adams RH, et al. Roles of ephrinB ligands and EphB receptors in cardiovascular development: demarcation of arterial/venous domains, vascular morphogenesis, and sprouting angiogenesis. *Genes Dev.* 1999;13(3):295–306.

22. Gerety SS, Wang HU, Chen ZF, Anderson DJ. Symmetrical mutant phenotypes of the receptor EphB4 and its specific transmembrane ligand ephrin-B2 in cardiovascular development. *Mol Cell.* 1999;4(3):403–414.

23. Wang HU, Chen ZF, Anderson DJ. Molecular distinction and angiogenic interaction between embryonic arteries and veins revealed by ephrin-B2 and its receptor Eph-B4. *Cell.* 1998;93(5):741–753.

24. Swift MR, Weinstein BM. Arterial-venous specification during development. *Circ Res.* 2009; 104(5):576–588.

25. Cowan CA, et al. Ephrin-B2 reverse signaling is required for axon pathfinding and cardiac valve formation but not early vascular development. *Dev Biol.* 2004;271(2):263–271.

26. Makinen T, et al. PDZ interaction site in ephrinB2 is required for the remodeling of lymphatic vasculature. *Genes Dev.* 2005;19(3):397–410.

27. Foo SS, et al. Ephrin-B2 controls cell motility and adhesion during blood-vessel-wall assembly. *Cell.* 2006;124(1):161–173.

28. Anand S, et al. MicroRNA-132-mediated loss of p120RasGAP activates the endothelium to facilitate pathological angiogenesis. *Nat Med.* 2010;16(8):909–914.

29. Pelster B, Burggren WW. Disruption of hemoglobin oxygen transport does not impact oxygen-dependent physiological processes in developing embryos of zebra fish (Danio rerio). *Circ Res.* 1996; 79(2):358–362.

30. Barrionuevo WR, Burggren WW. O2 consumption and heart rate in developing zebrafish (Danio rerio): influence of temperature and ambient O2. *Am J Physiol.* 1999;276(2 pt 2):R505–R513.

31. Ekker SC. Morphants: a new systematic vertebrate functional genomics approach. *Yeast.* 2000; 17(4):302–306.

32. Lawson ND, Weinstein BM. In vivo imaging of embryonic vascular development using transgenic zebrafish. *Dev Biol.* 2002;248(2):307–318.

33. Traver D, Paw BH, Poss KD, Penberthy WT, Lin S, Zon LI. Transplantation and in vivo imaging of multilineage engraftment in zebrafish bloodless mutants. *Nat Immunol.* 2003;4(12):1238–1246.

34. Isogai S, Horiguchi M, Weinstein BM. The vascular anatomy of the developing zebrafish: an atlas of embryonic and early larval development. *Dev Biol.* 2001;230(2):278–301.

35. Choi J, et al. Aplexone targets the HMG-CoA reductase pathway and differentially regulates arteriovenous angiogenesis. *Development.* 2011; 138(6):1173–1181.

36. Tong J, Elowe S, Nash P, Pawson T. Manipulation of EphB2 regulatory motifs and SH2 binding sites switches MAPK signaling and biological activity. *J Biol Chem.* 2003;278(8):6111–6119.

37. Isogai S, Lawson ND, Torrealday S, Horiguchi M, Weinstein BM. Angiogenic network formation in the developing vertebrate trunk. *Development.* 2003;130(21):5281–5290.

38. Roman BL, et al. Disruption of acvrl1 increases endothelial cell number in zebrafish cranial vessels. *Development.* 2002;129(12):3009–3019.

39. Guertin DA, Sabatini DM. Defining the role of mTOR in cancer. *Cancer Cell.* 2007;12(1):9–22.

40. Zygmunt T, et al. In parallel interconnectivity of the dorsal longitudinal anastomotic vessels requires both VEGF signaling and circulatory flow. *J Cell Sci.* 2012;125(pt 21):5159–5167.

41. Junttila TT, et al. Ligand-independent HER2/HER3/PI3K complex is disrupted by trastuzumab and is effectively inhibited by the PI3K inhibitor GDC-0941. *Cancer Cell.* 2009;15(5):429–440.

42. Serra V, et al. NVP-BEZ235, a dual PI3K/mTOR inhibitor, prevents PI3K signaling and inhibits the growth of cancer cells with activating PI3K mutations. *Cancer Res.* 2008;68(19):8022–8030.

43. Verheijen JC, Zask A. Phosphatidylinositol 3-kinase (PI3K) inhibitors as anticancer drugs. *Drugs Fut.* 2007;32(6):537–547.

44. Yan L, Findlay GM, Jones R, Procter J, Cao Y, Lamb RF. Hyperactivation of mammalian target of rapamycin (mTOR) signaling by a gain-of-function mutant of the Rheb GTPase. *J Biol Chem.* 2006;281(29):19793–19797.

45. Li Y, Corradetti MN, Inoki K, Guan KL. TSC2: filling the GAP in the mTOR signaling pathway. *Trends Biochem Sci.* 2004;29(1):32–38.

46. Kawakami K. Transgenesis and gene trap methods in zebrafish by using the Tol2 transposable element. *Methods Cell Biol.* 2004;77:201–222.

47. Kawakami K. Transposon tools and methods in zebrafish. *Dev Dyn.* 2005;234(2):244–254.

48. Kawakami K. Tol2: a versatile gene transfer vector in vertebrates. *Genome Biol.* 2007;8(suppl 1):S7.

49. Kwan KM, et al. The Tol2kit: a multisite gateway-based construction kit for Tol2 transposon transgenesis constructs. *Dev Dyn.* 2007; 236(11):3088–3099.

50. Pamonsinlapatham P, et al. P120-Ras GTPase activating protein (RasGAP): a multi-interacting protein in downstream signaling. *Biochimie.* 2009; 91(RasGAP):320–328.

51. Scheffzek K, et al. The Ras-RasGAP complex: structural basis for GTPase activation and its loss in oncogenic Ras mutants. *Science.* 1997; 277(5324):333–338.

52. Pylayeva-Gupta Y, Grabocka E, Bar-Sagi D. RAS oncogenes: weaving a tumorigenic web. *Nature reviews Cancer.* 2011;11(11):761–774.

53. Johnson GL, Vaillancourt RR. Sequential protein kinase reactions controlling cell growth and differentiation. *Curr Opin Cell Biol.* 1994;6(2):230–238.

54. Rodriguez-Viciana P, et al. Phosphatidylinositol-3-OH kinase as a direct target of Ras. *Nature.* 1994;370(6490):527–532.

55. Rodriguez-Viciana P, Marte BM, Warne PH, Downward J. Phosphatidylinositol 3′ kinase: one of the effectors of Ras. *Philos Trans R Soc Lond B Biol Sci.* 1996;351(1336):225–231.

56. Rodriguez-Viciana P, Warne PH, Vanhaesebroeck B, Waterfield MD, Downward J. Activation of phosphoinositide 3-kinase by interaction with Ras and by point mutation. *EMBO J.* 1996;15(10):2442–2451.

57. Castellano E, Downward J. RAS interaction with PI3K: more than just another effector pathway. *Genes Cancer.* 2011;2(3):261–274.

58. Kim YH, Hu H, Guevara-Gallardo S, Lam MT, Fong SY, Wang RA. Artery and vein size is balanced by Notch and ephrin B2/EphB4 during angiogenesis. *Development.* 2008;135(22):3755–3764.

59. Herbert SP, et al. Arterial-venous segregation by selective cell sprouting: an alternative mode of blood vessel formation. *Science.* 2009; 326(5950):294–298.

60. Davis S, et al. Ligands for EPH-related receptor tyrosine kinases that require membrane attachment or clustering for activity. *Science.* 1994; 266(5186):816–819.

61. Lam C, Bouffet E, Tabori U, Mabbott D, Taylor M, Bartels U. Rapamycin (sirolimus) in tuberous sclerosis associated pediatric central nervous system tumors. *Pediatr Blood Cancer.* 2010;54(3):476–479.

62. Hammill AM, et al. Sirolimus for the treatment of complicated vascular anomalies in children. *Pediatr Blood Cancer.* 2011;57(6):1018–1024.

63. Mammoto A, et al. A mechanosensitive transcriptional mechanism that controls angiogenesis. *Nature.* 2009;457(7233):1103–1108.

64. Connor KM, et al. Quantification of oxygen-induced retinopathy in the mouse: a model of vessel loss, vessel regrowth and pathological angiogenesis. *Nat Protoc.* 2009;4(11):1565–1573.

65. Minami M, Koyama T, Wakayama Y, Fukuhara S, Mochizuki N. EphrinA/EphA signal facilitates insulin-like growth factor-I-induced myogenic differentiation through suppression of the Ras/extracellular signal-regulated kinase 1/2 cascade in myoblast cell lines. *Mol Biol Cell.* 2011; 22(18):3508–3519.

66. Lin KT, Sloniowski S, Ethell DW, Ethell IM. Ephrin-B2-induced cleavage of EphB2 receptor is mediated by matrix metalloproteinases to trigger cell repulsion. *J Biol Chem.* 2008;283(43):28969–28979.

67. Ma L, et al. Identification of S664 TSC2 phosphorylation as a marker for extracellular signal-regulated kinase mediated mTOR activation in tuberous sclerosis and human cancer. *Cancer Res.* 2007;67(15):7106–7112.

68. Chan J, et al. Morphogenesis of prechordal plate and notochord requires intact Eph/ephrin B signaling. *Dev Biol.* 2001;234(2):470–482.

69. Chan J, Bayliss PE, Wood JM, Roberts TM. Dissection of angiogenic signaling in zebrafish using a chemical genetic approach. *Cancer Cell.* 2002;1(3):257–267.